

COMPARISON BETWEEN ALTERNATIVE FE MODELLING STRATEGIES FOR RIVETED CONNECTIONS CONCERNING FATIGUE ASSESSMENTS

M.P.G. Rodrigues¹; A.M.P. de Jesus^{1,2}; A.L.L. Silva¹

¹Unidade de Concepção e Validação Experimental, IDMEC, Pólo FEUP, Porto, Portugal

²Departamento de Engenharias, Escola de Ciências e Tecnologia, Universidade de Trás-os-Montes e Alto Douro, Vila Real, Portugal



ABSTRACT

Nowadays, fatigue assessment of ancient riveted metallic bridges has deserved special attention. Despite those structures are reaching the end of their lifecycle, their replacement in a short period is economically unsustainable. Therefore, more research is required to better understand the behaviour of riveted bridges, in particular the fatigue behaviour of their riveted connections, in order to circumstantiate any decision regarding the extension of their life cycle. Riveted bridges were manufactured connecting angles and plates using rivets. Multiple rivet joints are typical in those structures. This paper presents a methodology, based on the finite element analysis, to assess the local stresses in multiple rivet connections, taking into account friction and clamping stresses on rivets. In particular, stress concentration factors for uncracked connections are evaluated as well as the stress intensity factors for several crack configurations. The stress intensity factors are evaluated using the virtual crack closure technique.

1. INTRODUÇÃO

At the end of the 19th century and beginning of 20th century, many metallic riveted road and railway bridges were built. A significant number of those bridges are still in operation. Their maintenance and safety is a major concern of governmental agencies, since these bridges were designed taking into account traffic conditions completely different from those observed nowadays. In order to assure high safety levels in old riveted steel bridges, highway and railway authorities have to invest heavily in their maintenance and retrofitting.

The design procedures were not yet fully developed or even did not exist in the 19th century and design engineers were not aware

of some important phenomena such as fatigue. The fatigue phenomenon was only intensively studied in the 20th century. A number of fatigue assessment methodologies for riveted railway bridges have been proposed. The S-N approach is widely used to assess the fatigue damage for riveted steel constructions (DiBattista *et al.* 1998, Geissler 2002, Kulak 2000, Kim *et al.* 2001). Fracture Mechanics appears as an alternative approach to perform residual life calculations (Wang *et al.* 2006, Paasch & DePiero 1999). However, the use of the Fracture Mechanics is very often limited to the application of simplified formulae for stress intensity factors evaluation, available in standard handbooks (Tada *et al.* 2000). For example, the stress intensity factor in a cracked plate is calculated by considering an isolated

plate rather than a plate integrated in a riveted structural member. No interaction is taken into account between the cracked plate and the remaining components of the member. This may result in inconsistent residual life evaluations, motivating the search for more accurate stress intensity factor solutions.

Local stress/strain approaches may also be used to assess the fatigue life of riveted connections. This approach requires detailed local stress/strain analyses at the level of the riveted connections. There are only few cases where detailed 3D finite element models have been used in stress analysis of uncracked riveted connections (DePiero *et al.* 2002, Al-Emrani & Kliger 2003, Imam 2006, Imam *et al.* 2007, Righiniotis *et al.* 2008, De Jesus *et al.* 2010).

This paper proposes a comparison of two alternative finite element modelling strategies for riveted connections, which may be used for fatigue assessments. In the first approach, the plates of the connection are modelled using solid finite elements; the second approach uses shell finite elements. The second modelling approach may be convenient if a reduction in computation effort is required. Based on proposed finite element models, some riveted connections are analysed to assess the local stresses, namely the elastic stress concentration factors for uncracked geometries and the stress intensity factors, for cracked geometries. The stress intensity factors are evaluated using the virtual crack closure technique (VCCT technique) (Krueger 2004). The effects of friction and clamping stresses on rivets are accounted in the models. A single rivet and multiple rivet joints, with distinct rivet configurations are analysed.

Fig. 1 presents a categorization of riveted constructional details with respect to fatigue behaviour as proposed by Taras & Greiner (2010). Detail category 3, which corresponds to symmetrical spliced riveted joints under tensile loading, is considered in the current investigation. The effects of the number of rows of rivets along and perpendicular to the loading direction are investigated.

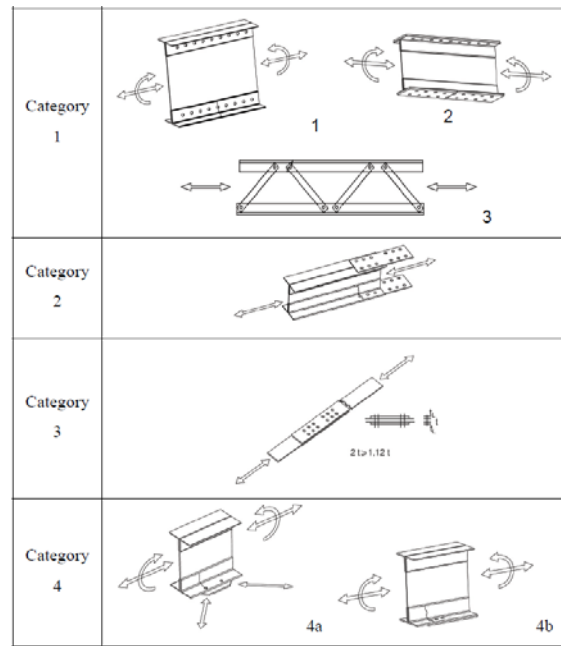


Fig. 1 – Categorization of riveted constructional details with respect to fatigue behaviour (Taras & Greiner, 2010).

2. FINITE ELEMENT MODELLING OF RIVETED CONNECTIONS

The elastic stress concentration factor was determined for three distinct connections, namely a single rivet joint, a 1×4 matrix riveted joint and finally a 2×2 matrix riveted joint. The 1×4 matrix rivet configuration is proposed to investigate the evolution of the stress concentration on rivet holes placed along the loading line. The 2×2 matrix rivet allows the investigation of the stress concentration evolution along a line perpendicular to loading. The 2×2 matrix riveted joint was also used for stress intensity factor computations. For all cases, two finite element models, with solid and shell elements were proposed. These models were built using the ANSYS[®] software, with ANSYS[®] parametric design language – APDL language (SAS, 2008).

A class of models was proposed using solid elements to represent the rivet and the plates of the connection. For these models, the rivet and the plates were modelled using hexahedra isoparametric 20-noded elements (SOLID95). The contact between the rivet and plate members was modelled through contact elements available in ANSYS[®],

using a surface-to-surface option. In particular, the CONTA174 and TARGE170 elements were used to model, respectively, the contact and target surfaces, forming the so-called contact pair. Both surfaces in contact were assumed flexible.

Another class of models using shell elements to model the plates of the connection was proposed. The rivets still are modelled using SOLID95 elements. Two types of shell elements were tested, namely with 4 nodes (SHELL63) and 8 nodes (SHELL93). The contact pairs between surfaces were modelled using the CONTA174 and TARGE170 elements. The contact between the shell and rivet shoulder was modelled using the CONTA175 and TARGE170 elements.

Materials were considered linear elastic and isotropic ($E=210$ GPa; $\nu=0.27$). Even considering a linear behaviour of the materials, the analysis was non-linear because of the contact. Therefore, an incremental analysis was used.

All simulations were performed using the augmented Lagrange contact algorithm, together with de Coulomb friction model. The augmented Lagrange algorithm requires the definition of the normal contact stiffness. The amount of penetration between two contacting surfaces (contact and target) depends on the normal stiffness. High values of normal stiffness decrease the amount of penetration, but may lead to numerical instabilities and convergence difficulties. Low values of normal stiffness provide high penetration, decreasing the accuracy of the solution. Ideally, it is desirable a high enough normal stiffness value to provide a lower level of penetration, but low enough to provide convergence. The contact stiffness is responsible for the contact pressure between contacting surfaces. The contact pressure is directly linked to the product of the contact stiffness (κ) and penetration (δ). The penetration level, δ , is dependent of the normal stiffness κ . Null penetration would require $\kappa=\infty$, therefore leading to numerical instabilities. The κ value assumed by ANSYS® depends on the relative stiffness

between the two bodies in contact, being possible to scale κ by the FKN factor, usually called the normal penalty stiffness factor. The usual FKN range is within 0.01 and 1.0, with the ANSYS® default, $FKN=1.0$ (SAS, 2008).

Another important parameter on the augmented Lagrange contact algorithm is the FTOLN parameter. This parameter defines the penetration tolerance, along the normal direction of the contact surface. The usual range for this parameter is lower than 1.0 (usually less than 0.2), being the default value of 0.1 (SAS, 2008). This parameter is used to evaluate if the penetration compatibility condition is satisfied. The penetration compatibility is satisfied if penetration is within the admissible value (FTOLN times the depth of underlying elements). If the penetration is higher than the admissible value, more iterations are necessary, even the residual forces meet the convergence requirements.

Null clearance between the riveted holes was considered, because this is characteristic of riveted connections. The clamping stress effect of the rivet was taken into account in this study. The clamping was modelled setting a preliminary load step consisting of a temperature variation (ΔT) and defining orthotropic thermal expansion properties for the rivet: nonzero thermal expansion coefficient on the axial direction of the rivet ($\alpha=10^{-5}$ °C⁻¹) and null thermal expansion on the transversal plane of the rivet. Despite inspired on the riveting process, the application of a temperature variation to the rivet was only used as an analytical methodology to generate clamping stresses. The actual clamping stresses on rivets of existing connections are not easy to quantify. On this context, the single rivet model is used to make a sensitivity analysis, to evaluate the influences of several values of clamping stresses on the stress distribution around the rivet hole. When the clamping stress is taken in account, the friction effect is significant on the local stress distribution.

The exact value of friction coefficient is difficult to evaluate. The friction value of

0.3 has been used in simulation of riveted joints by several authors such as Al-Emrani & Kliger (2003), Moreno & Valiente (2006), Imam (2006), Imam *et al.* (2007). Paasch & DePiero (1999) considered a friction coefficient changing from 0.0 to 0.5. They also refer that static and sliding coefficients of friction for mild steel on mild steel are 0.74 and 0.57 respectively. Eurocode 3 suggests, for joints design, slip factors in the range of 0.2–0.5 (CEN, 2004). In this paper, a friction coefficient of 0.3 was adopted in all simulations, since this value has been assumed as a reference value in the literature. Furthermore, variations in the friction coefficient were also simulated in order to provide some sensibility analysis of the stress field to the friction coefficient.

3. ELASTIC STRESS CONCENTRATION FACTOR EVALUATION

The elastic stress concentration factor was defined as the ratio between the maximum stress at the surface of the rivet hole, in the loading direction, and the uniform net stress, evaluated in the plate cross section containing the rivet axis and is normal to the loading.

3.1- Finite solid element models

3.1.1- *Single rivet joint*

A single rivet connection was modelled in this study. The geometry of the single rivet connection is shown in Fig. 2. The connection model is only $\frac{1}{4}$ of the total geometry, taking advantages of the two planes of symmetry of the connection (Fig.3). Nodes at the planes of symmetry were restrained in the normal direction. The AB surface (Fig. 2) was subjected to a uniform displacement of 0.1 mm, along the longitudinal direction.

Fig. 4 illustrates the clamping stresses as a function of the temperature range applied to the rivet (0, 25, 75, 125, 175, 225 and 275 °C) for several FKN factors (1.0, 0.1 and 0.01), friction coefficients, μ (0.0, 0.3 and 0.6) and FTOLN=0.1. Fig. 4 shows that the

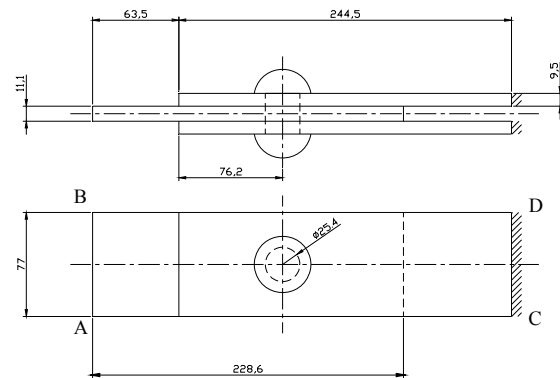


Fig. 2 – Geometry of the single rivet connection (dimensions in mm).

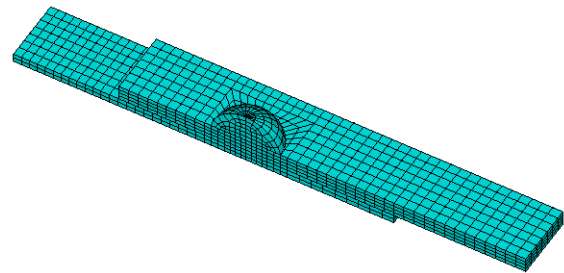


Fig. 3 – Finite element mesh of the single rivet joint, using solid elements: $\frac{1}{4}$ of the total geometry.

clamping stress increases linearly with the temperature range. The FKN factor has a significant influence of the clamping stress. The friction coefficient has almost no effect on clamping stress. In Fig. 4 and in all figures reporting numerical results, symbols stand for numerical results from individual simulations.

Fig. 5 shows the evolution of the elastic stress concentration factor with the clamping stress, FKN factor and friction (FTOLN=0.1). The elastic stress concentration factor decreases with increasing of the clamping stress. For FKN=1.0 or FKN=0.1 and non-null friction, the elastic stress concentration tends to the unity as the clamping stress increases, which is a physically consistent behaviour. Without friction, load transfers exclusively by bearing; the combination of friction and clamping stresses increases the load transfer through friction, reducing the load transfer by bearing, thus reducing the elastic stress concentration factor.

Taking into account the discussion about Fig. 5, simulations for the other riveted geometries will be carried out using FKN=1.0, which corresponds to the ANSYS default.

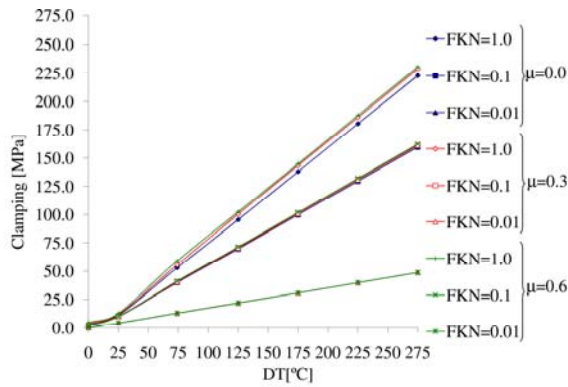


Fig. 4 – Evolution of the clamping stress with the temperature variation applied to the rivet: solid model.

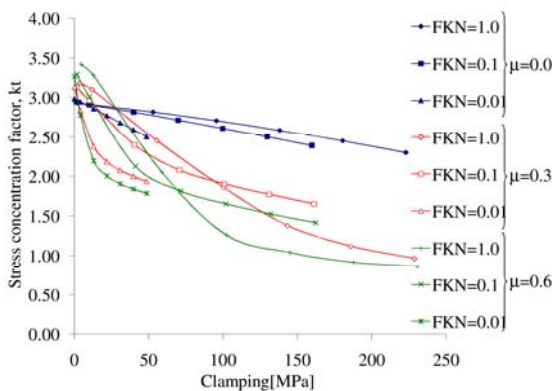


Fig. 5 – Evolution of the elastic stress concentration factor with the clamping stress, FKN and friction (solid model).

3.1.2- Multiple rivet joint: 1×4 matrix of rivets

Fig. 6 illustrates a multiple rivet connection with a base 1×4 rivet matrix. Two planes of symmetry were assumed, namely faces AC and DC (see Fig. 6). Therefore, the proposed model represents a connection with 16 rivets: two rows of 8 rivets each. Fig. 7 shows the finite element mesh of the connection. Null displacements were assumed in the planes of symmetry along the normal direction; additionally, a displacement of 0.1 mm was applied to the AB face, along the longitudinal direction.

Fig. 8 illustrates the evolution of the elastic stress concentration factor with the clamping stress for two friction coefficients, $\mu=0.3$ and $\mu=0.6$ (FKN=1.0; FOLTN=0.1). The elastic stress concentration factor decreases with the increase of the clamping stress. The stress concentration factor is higher for the first rivet, near the end of the

overlapping plate, and reduces significantly as the distance of the rivet to the end increases. For rivets 3 and 4 there are almost no stress concentration. The friction reduces the stress concentration for intermediate/high clamping stresses; for low clamping stresses, this effect is reversed. The friction effect is more sensible for the first rivet, near the end of the overlapping plate, and fades as the distance of the rivet to the end increases.

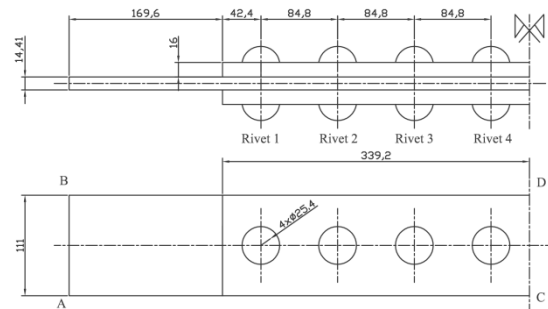


Fig. 6 – Geometry of a multiple rivet connection: 1×4 matrix of rivets (dimensions in mm).

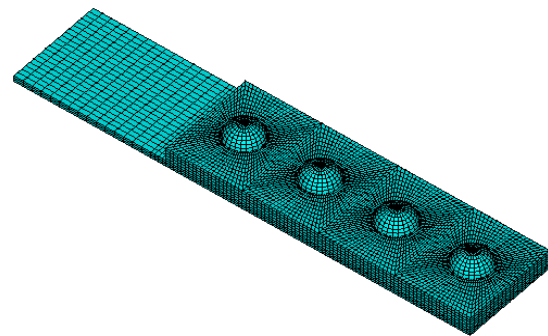


Fig. 7 – Finite element model of a multiple rivet connection, using finite solid elements: 1×4 matrix of rivets (1/8 of the geometry).

3.1.3- Multiple rivet joint: 2×2 matrix of rivets

Fig. 9 illustrates the geometry of a multiple rivet connection with a 2×2 matrix of rivets. Faces AC and DC are assumed planes of symmetry. Therefore, the proposed finite element model represents a riveted connection with 4 rows of 4 rivets each. Fig. 10 shows the finite element mesh of the connection. The boundary conditions are the same as in the previous connection.

The Fig. 11 shows the evolution of the elastic stress concentration factor with the clamping stress and friction (FKN=1.0; FTOLN=0.1). In the same way as observed in

the previous analyses, the stress concentration factor decreases with the clamping stress. Also, the elastic stress concentration is higher for the rivets near the end/side of the overlapping plates (rivet 2, $k_t > 3.5$). In the perspective of a fatigue assessment, rivet 2 is the most critical. Fig. 11 also shows that k_t is higher for the lower friction, for low clamping stresses. However, this observation is reversed for high clamping stress values.

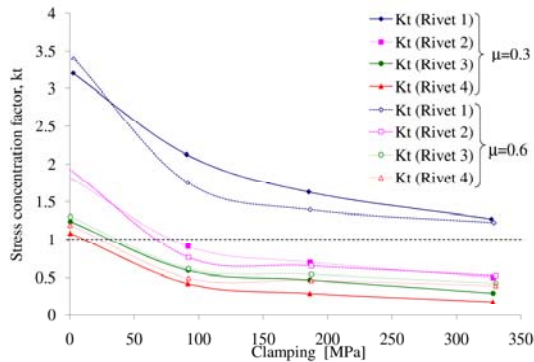


Fig. 8 – Evolution of the elastic stress concentration factor with the clamping stress and friction (μ) for the multiple rivet connection: 1x4 matrix of rivets (solid model).

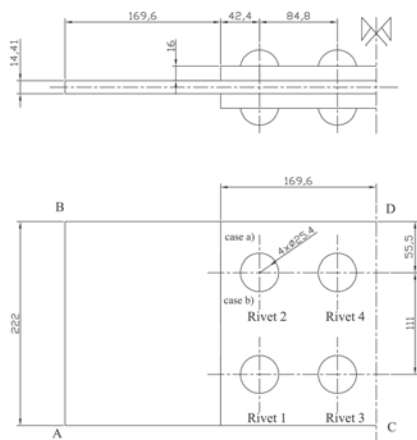


Fig. 9 – Geometry of a multiple rivet connection: 2x2 matrix of rivets (dimensions in mm).

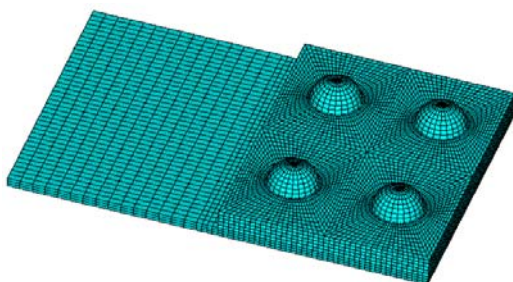


Fig. 10 – Finite element model of a multiple rivet connection, using finite solid elements: 2x2 matrix of rivets (1/8 of the geometry).

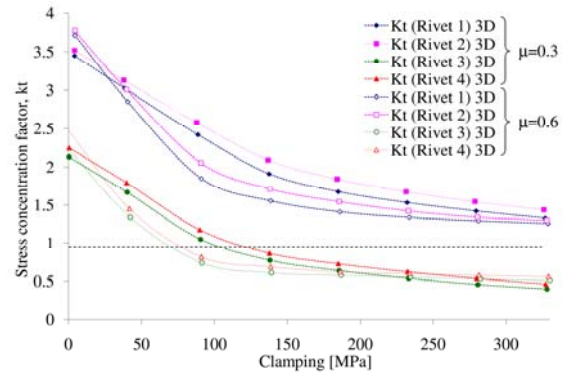


Fig. 11 – Evolution of the elastic stress concentration factor with the clamping stress and friction (μ) for the multiple rivet connection: 2x2 matrix of rivets (solid model).

3.2- Finite shell element models

This section presents results of the elastic stress concentration factor for the same riveted connections investigated in section 3.1, but now with the plates of the connection modelled with finite shell elements.

3.2.1- Single rivet joint

The single rivet connection shown in the Fig. 2 is modelled using finite shell elements for the plates and solid elements for the rivet. Only $\frac{1}{2}$ of the connection is modelled, as illustrated in the finite element mesh of Fig. 12. Displacements normal to the symmetry plane are restrained, as well as rotations along the edges direction of the plates, in the symmetry plane.

Fig. 13 shows the evolution of the clamping stress with the temperature range (25, 125, 225, 300, 500, 750, 1000 and 1500 °C), FKN (1.0, 0.1, 0.01) and μ (0.0, 0.3, 0.6), for two types of shell elements (4- and 8-noded elements, respectively SHELL63 and SHELL93). Both elements exhibited very similar responses. In order to achieve similar clamping stresses, as simulated in the solid models, significantly higher temperature variations have to be applied, as demonstrated by the simulations. It appears that shell models have lower bending stiffness than solid elements based models.

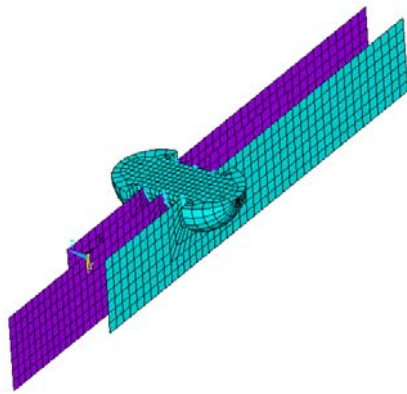


Fig. 12 – Finite element mesh of the single rivet joint, using shell elements: 1/2 of the total geometry.

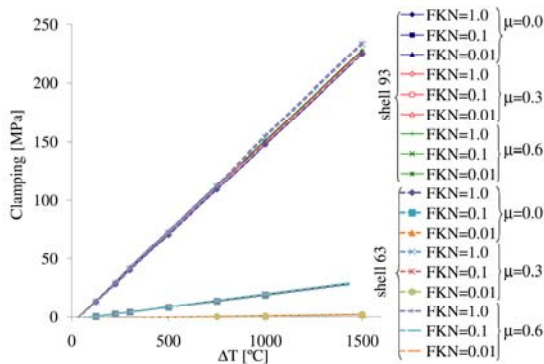


Fig. 13 – Evolution of the clamping stress with the temperature variation applied to the rivet: shell model.

Fig. 14 shows the evolution of the elastic stress concentration factor with the clamping stress, FKN factor (1.0, 0.1 and 0.01) and friction (0.3, 0.6). FTOLN was set to 0.1, the ANSYS® default. The trend between the stress concentration factor and the clamping stress verified for the solid models is again confirmed in this model. The FKN parameter has a significant effect on stress concentration. The FKN equal to the unity seems to be a proper choice, since the clamping stress develops easily. The curves seem to tend for a stabilised stress concentration factor above the unity. Results obtained using the SHELL93 element (8-noded element) is slightly higher than results obtained using the SHELL63 element (4-noded element).

Comparing the results from section 3.1.1 with results from this section, it is clear that solid models predicted higher stress concentration factors for null/low clamping stresses.

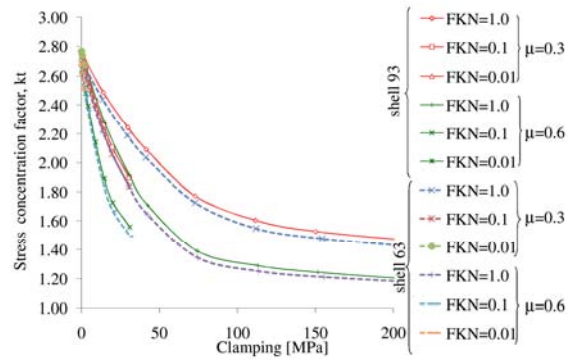


Fig. 14 – Evolution of the elastic stress concentration factor with the clamping stress, FKN and friction (shell elements).

3.2.2- Multiple rivet joint: 1x4 matrix of rivets

Fig. 15 shows the finite element mesh, with shell elements, of a multiple rivet joint with a 1x4 matrix of rivets. This model represents a 16 rivets connection, due to two planes of symmetry, as described in the section 3.1.2.

Fig. 16 shows the evolution of the elastic stress concentration factor for all rivets, as a function of the clamping stress and friction (FKN=1.0; FTOLN=0.1). Fig. 16 shows similar trends as observed for the corresponding solid model. Again, the closest rivet to the end of the cover plate is the more stressed one. The rivet more distant from that end do not show any stress concentration at all. Friction increasing produces always stress concentration reduction.

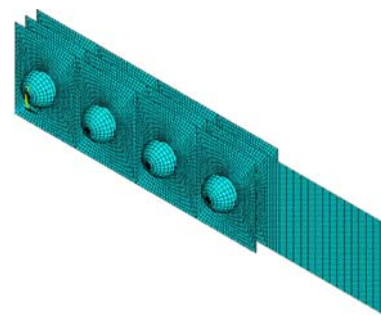


Fig. 15 - Finite element model of a multiple rivet connection, using finite shell elements: 1x4 matrix of rivets (1/4 of the geometry).

Fig. 17 provides a comparison between solid and shell model predictions for the case of the multiple rivet connection with a 1x4 matrix of rivets. The elastic stress concentration factor from the shell model is always

lower than stress concentration from the solid model, for the first rivet (nearest from the cover plate end) ($\mu=0.3$ and $\mu=0.6$). For the others rivets this behaviour is reversed, the k_t from the shell model being higher than the k_t from the solid model.

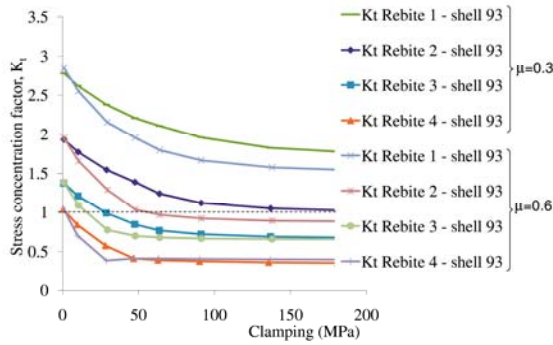


Fig. 16 - Evolution of the elastic stress concentration factor with the clamping stress and friction (μ) for the multiple rivet connection: 1x4 matrix of rivets (shell model).

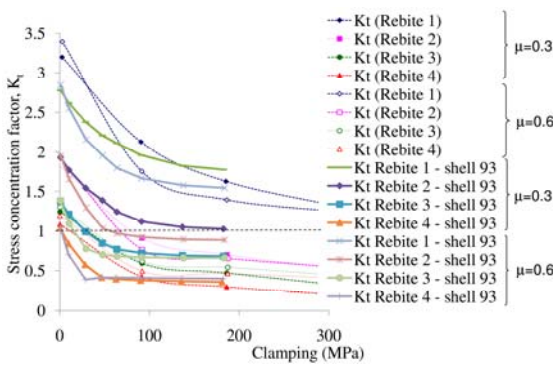


Fig. 17 – Comparison of the stress concentration factor between solid and shell models: 1x4 matrix of rivets.

3.2.3- Multiple rivet joint: 2x2 matrix of rivets

The multiple rivet connection referred in section 3.1.3 was modelled using shell elements to represent the plates. Fig. 18 illustrates the finite element mesh. Rivets were modelled using solid elements. The model represented in Fig. 18 corresponds to a connection of 16 rivets since symmetry boundary conditions were applied. Fig. 19 shows the evolution of the elastic stress concentration factor with the clamping stress and friction ($FKN=1.0$; $FTOLN=0.1$). For this case, only rivet 3 exhibit a stress concentration factor lower than unity for high clamping and $\mu=0.6$. Rivet 2, which is the rivet closest both to the end and to the side of the cover plates, is the one with highest stress concentration.

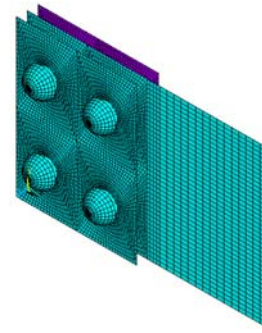


Fig. 18 – Finite element model of a multiple rivet connection, using finite shell elements: 2x2 matrix of rivets (1/4 of the geometry).

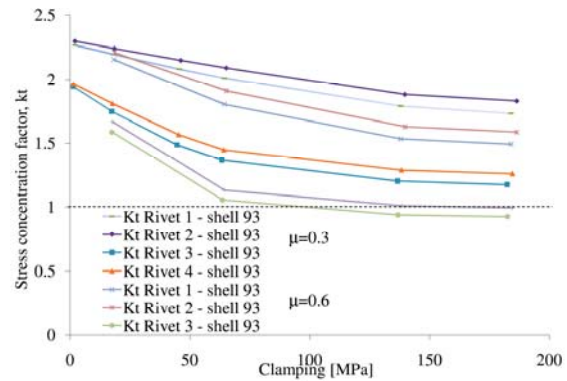


Fig. 19 – Evolution of the elastic stress concentration factor with the clamping stress and friction (μ) for the multiple rivet connection: 2x2 matrix of rivets (shell model).

Fig. 20 provides a comparison for elastic stress concentration factors between shell and solid models. For low clamping stresses (<75 MPa), solid model yields higher stress concentration factors than shell models. However, for high clamping stresses, the shell model tends to produce the highest stress concentration values.

4. STRESS INTENSITY FACTOR EVALUATION

Stress intensity factors for a propagating crack, emanating from a rivet hole, are computed for the multiple rivet connection, with a 2x2 matrix of rivets. Two types of crack configurations (configuration a) and configuration b)) were defined, as illustrated in Fig. 21. Both cracks were assumed to start from rivet 2, since it exhibited the highest stress concentration factors. The crack configuration b) is assumed to appear after crack configuration a) reaches the side of the plate. Cracks were

assumed to propagate only in the connection middle plate.

Stress intensity factors were evaluated using the virtual crack closure technique. Both solid and shell models were used to compute the stress intensity factors. The same contact parameters were used in these analyses, as defined in sections 3.1.3 and 3.2.3. Two distinct clamping stresses were used in the analyses. These clamping stresses were generated in the shell and solid models adjusting the temperature variation applied to the rivets, using results of preliminary simulations, in order to result the same clamping stresses in solid and shell models. Since the clamping stresses have a significant influence on local stress distributions, the comparison between the two types of finite element models must be based on the same clamping stresses.

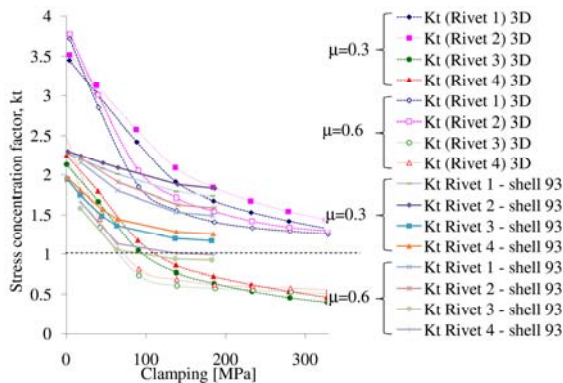


Fig. 20 – Comparison of the stress concentration factor between solid and shell models: 2x2 matrix of rivets.

4.2. Finite solid element models

Cracks were generated in the finite element model described in section 3.1.3. The same mesh was used, but coincident nodes were placed in the location of the crack. Fig. 22 shows the two crack configurations considered in this analysis.

Fig. 23 and 24 shows the evolution of the stress intensity factor with the crack length (configuration a)), for the finite solid element model, for a clamping stress of 20.3 MPa (Fig. 23) and 89.2 MPa (Fig. 24). Fig. 25 and 26 shows the evolution of the stress intensity factor with the crack length,

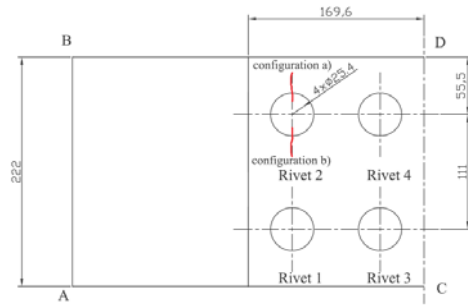


Fig. 21 – Two configurations of cracks emanating from rivet 2.

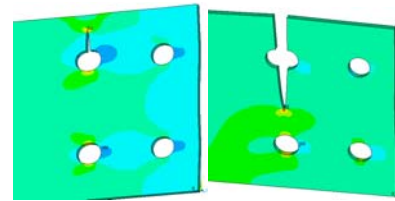


Fig. 22 – Cracks on the multiple rivet connection with a 2x2 matrix of rivets (solid model): crack configurations a) (left) and b) (right).

for the crack configuration b), for a clamping stress of 20.3 MPa and 89.2 MPa, respectively. All graphs include the maximum stress intensity across the plate thickness as well as the averaged value. The stress intensity factors were normalised using the average net stress in the middle plate. The numerical stress intensity factors were correlated using fifth order polynomials. Each graph gives the determination coefficient of those correlations.

Figs. 27 and 28 compare the stress intensity factor between the two clamping stresses, for both crack configurations. Higher clamping stresses result in lower stress intensity factors as would be expectable.

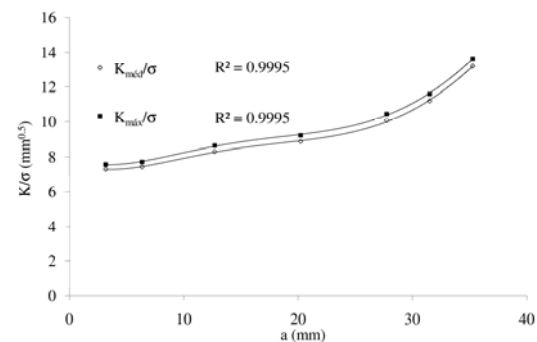


Fig. 23 – Evolution of the stress intensity factor with the crack length for the finite solid element model and for a clamping of 20.3 MPa: crack configuration a).

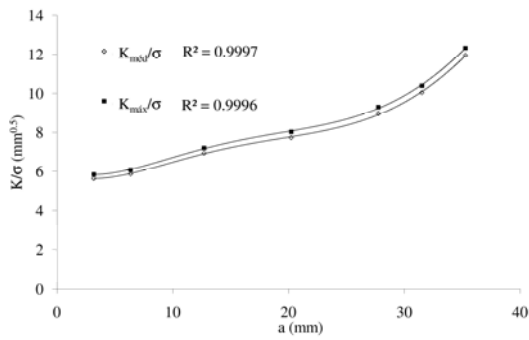


Fig. 24 – Evolution of the stress intensity factor with the crack length for the finite solid element model and for a clamping of 89.2 MPa: crack configuration a).

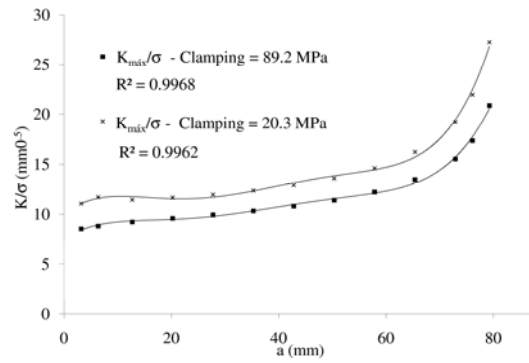


Fig. 28 – Comparison of the stress intensity factors obtained for the solid element model with two distinct clamping stresses: crack configuration b).

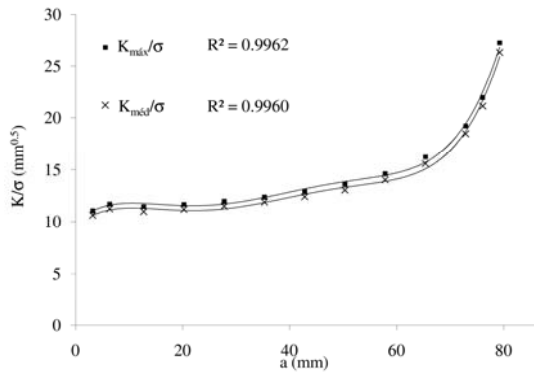


Fig. 25 – Evolution of the stress intensity factor with the crack length for the finite solid element model and for a clamping of 20.3 MPa: crack configuration b).

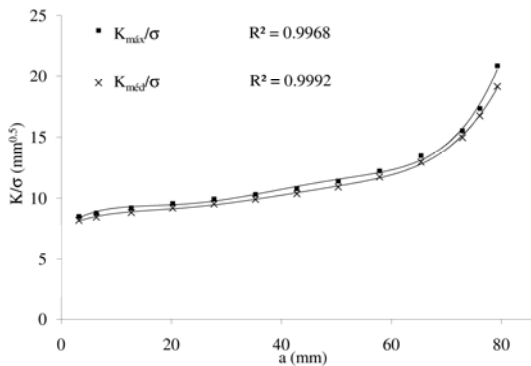


Fig. 26 – Evolution of the stress intensity factor with the crack length for the finite solid element model and for a clamping of 89.2 MPa: crack configuration b).

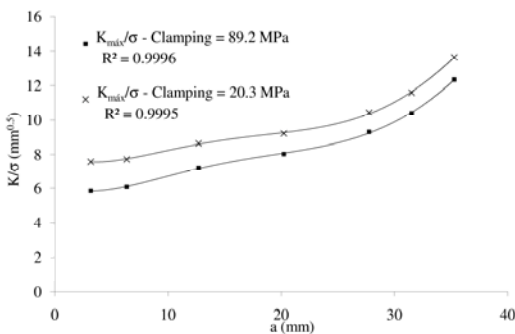


Fig. 27 – Comparison of the stress intensity factors obtained for the solid element model with two distinct clamping stresses: crack configuration a).

4.3. Finite shell element models

In this section, the cracked geometry investigated in the previous section, is now analysed using a shell model. The same crack configurations are analysed. Fig. 29 illustrates the two investigated cracks in the shell model. A 2D VCCT analysis was used to derive the stress intensity factors (Krueger 2004).

Figs. 30 and 31 show the evolution of the stress intensity factor for the two crack configurations, a) and b) respectively. In each graph, the beneficial effect of the clamping stress is illustrated: a stress intensity factor reduction is observed with increasing clamping stresses. The crack configuration b) shows significantly higher stress intensity factors. The stress intensity factors are noticeably high, since the normalized stress intensity factors are always above $20 \text{ mm}^{0.5}$, for cracks about 3mm in length. This means that for a net stress of 100 N/mm^2 results a minimum stress intensity of about $2000 \text{ N}\cdot\text{mm}^{-1.5}$ which is the same order of magnitude of the material toughness. A more refined analysis is required for smaller crack sizes in order to capture the stress intensity factors in early crack propagation, the more fatigue life consuming.

Fig. 32 and 33 compare of the stress intensity factor between shell and solid elements for both crack configurations. Both figures show that the stress intensity factors, obtained using the shell model, are higher than those obtained using the solid model. Roughly, the stress intensity factors

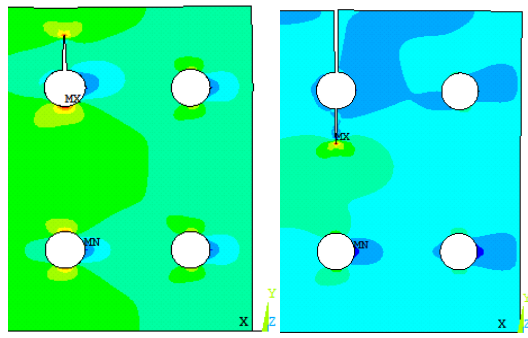


Fig. 29 – Cracks on the multiple rivet connection with a 2x2 matrix of rivets (shell model): crack configurations a) (left) and b) (right).

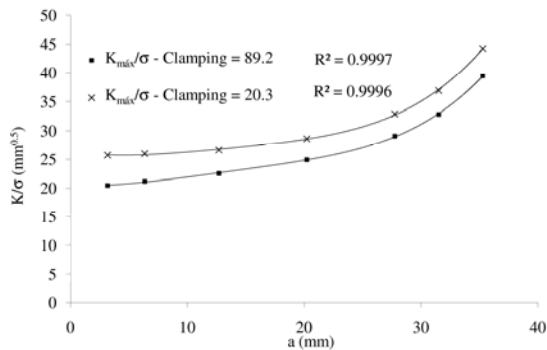


Fig. 30 – Evolution of the stress intensity factor with the crack length for the finite shell element model and for the clamping stresses of 20.3 MPa and 89.2 MPa: crack configuration a).

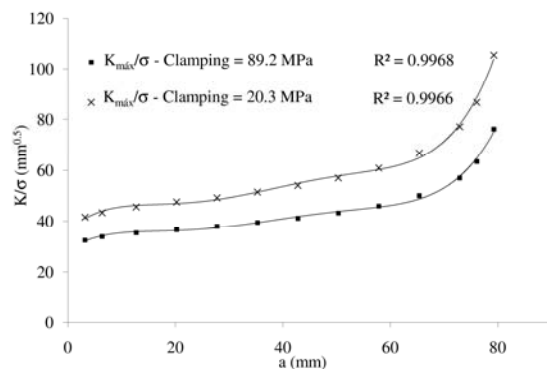


Fig. 31 – Evolution of the stress intensity factor with the crack length for the finite shell element model and for the clamping stresses of 20.3 MPa and 89.2 MPa: crack configuration b).

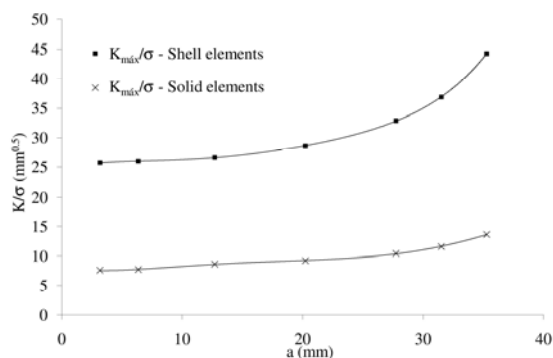


Fig. 32 – Comparison of stress intensity factors between shell and solid models for crack configuration a).

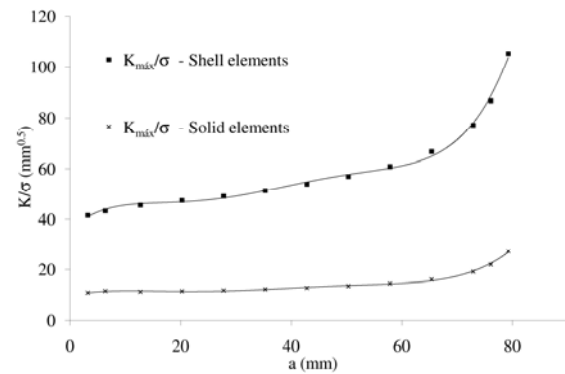


Fig. 33 – Comparison of stress intensity factors between shell and solid elements for crack configuration b).

from the shell model are 3 times higher than values from the solid model. It is interesting to note that regarding the stress intensity factor evaluation, the shell model predicts more critical values, but the situation is reversed if the stress concentration factor is analysed.

As far as authors are aware comparisons involving stress concentration factors and stress intensity factors between solid and shell models of riveted connections does not exist. However it is understood that shell models involves more simplification of the reality than solid models, therefore it is expected that results from shell models are poorer than results from solid models. The important advantage of the shell models, that may be claimed, is the lower computational cost they usually require. In the present case the shell models still requires significant computational costs since the nonlinearity from contact persists and the rivets still are modelled using solid elements. Nevertheless, Correia *et al.* (2010) have used results (k_t and K) from both shell and solid models of a single rivet connection to derive the global S-N curve of the referred riveted joint. The same conclusions were achieved, regarding the comparisons of the stress concentration and or crack configuration b).

model are 3 times higher than values from the solid model. It is interesting to note that g to note that regarding the stress intensity factor evacted higher crack initiation lives (lower k_t) but lower crack propagation lives (higher K), the final result being similar to the one obtained with the solid model.

5. CONCLUSIONS

This paper present the analysis of three riveted connections, namely with one rivet, 1×4 matrix of rivets and 2×2 matrix of rivets. Furthermore, two types of finite element models were tested, namely using shell and solid elements. The finite element models were built using contact finite elements that allowed the simulation of local effects such as friction combined with the clamping stresses on rivets. The simulations showed that ANSYS contact parameters defaults (FKN=1.0 and FTOLN=0.1) produced physically consistent results.

For multi-rivet connections, the most stressed rivets are those placed closest to the borders (end/side) of the overlapping plates. The stress concentration tends to reduce significantly as the distance (along the loading direction) to the end of the cover plate increases. Therefore, for a matrix of rivets, rivets from the border of the matrix are the one that need more attention concerning fatigue cracking.

The clamping stresses on rivets play a significant effect on stress concentration. High clamping stresses associated with friction tend to eliminate the stress concentration at rivets. However, rivets are generally characterized by low to moderate clamping stresses, which increases the load transfer by bearing resulting, consequently, in higher stress concentration on holes than observed in preloaded high strength bolted connections.

The comparison of results from solid and shell models highlighted significant differences both on stress concentration factors and stress intensity factors, mainly for low clamping stresses. The shell model resulted in lower elastic stress concentration factors and significantly higher stress intensity factors than observed in solid models.

5-ACKNOWLEDGEMENTS

The authors acknowledge the Portuguese Science Foundation for the support through the research project PTDC/EME-PME/78833/2006.

6-REFERENCES

- Al-Emrani, M., Kliger, R. 2003. FE analysis of stringer-to-floor-beam connections in riveted railway bridges, *Journal of Constructional Steel Research*, 59, p. 803-818.
- CEN, 2004, “Eurocode 3: Design of steel structures - Part 1-8: Design of joints”, European Committee for Standardization, Brussels.
- Correia, J.A.F.O., Jesus, A.M.P., Silva, A.L.L. 2010. Simulação por elementos finitos de curvas S-N de ligações rebitadas, 8º Congresso Nacional de Mecânica Experimental, Guimarães, 21-23 de Abril.
- De Jesus, A.M.P., Pinto, H., Fernández-Canteli, A., Castillo, E., Correia, J.A.F.O. 2010. Fatigue assessment of a riveted shear splice based on a probabilistic model, *International Journal of Fatigue*, 32, p. 453-462
- DePiero, A.H., Paasch, R.K., Lovejoy, S.C. 2002. Finite-element modeling of bridge deck connections details, *Journal of Bridge Engineering*, 7(4), p. 229-35.
- DiBattista J.D., Adamson D.E.J., Kulak G.L. 1998. Evaluation of remaining fatigue life for riveted truss bridges, *Canadian Journal of Civil Engineering*, 25(4) p. 678–91.
- Geissler K. 2002. Assessment of old steel bridges, Germany, *Structure Engineering International*, 12(4), p. 258–63.
- Imam B. 2006. Fatigue Analysis of Riveted Railway Bridges, Surrey: University of Surrey, p. 256, PhD Thesis.
- Imam, B.M., Righiniotis, T.D., Chryssanthopoulos, M.K. 2007. Numerical modelling of riveted railway bridge connections for fatigue evaluation, *Engineering Structures*, 29, p. 3071-3081.
- Kim, S.H., Lee, S.W., Mha, H.S. 2001. Fatigue reliability assessment of an existing steel railroad bridge, *Engineering Structures*, 23, p. 1203-1211.
- Krueger R. 2004. Virtual crack closure technique: history, approach, and applications, *Applied Mechanics Reviews*; 57(2), p. 109–43.
- Kulak, G. L. 2000. Fatigue strength of riveted shear splices, *Progress in Structural Engineering and Materials*, 2(1), p. 110-119.
- Moreno, J., Valiente, A., 2006, “Cracking induced failure of old riveted steel beams”, *Engineering Failure Analysis*, 13, p. 247–259

- Paasch, R.K., DePiero, A.H., 1999, "Fatigue crack modeling in bridge deck connection details", SPR 380, Final Report, Oregon State University, USA.
- Righiniotis, T.D., Imam, B.M., Marios K., Chryssanthopoulos, 2008. Fatigue analysis of riveted railway bridge connections using the theory of critical distances, *Engineering Structures*, 30, p. 2707-2715.
- SAS - Swanson Analysis Systems Inc. 2008. ANSYS, Houston, Version 11.0
- Tada, H., Paris. P.C., Irwin, G.R. 2000. *The stress analysis of cracks handbook*. ASME Press.
- Taras, A., Greiner, R., 2010, "Statistical Background to the Proposed Fatigue Class Catalogue for Riveted Components. Contribution to WG6.1 – Assessment of Existing Steel Structures", ECCS-TC6, Spring Meeting – Lausanne – March 22-23.
- Wang, C.S., Chen, A.R., Chen, W.Z., Xu, Y. 2006. Application of probabilistic fracture mechanics in evaluation of existing riveted bridges. *Bridge Structures*, 2(4), p. 223-232.